EUROPEAN COMMISSION

Horizon Europe Framework Programme (HORIZON)
HORIZON-EIC HORIZON EIC Grants

HORIZON Action Grant Budget-Based

GA No. 101070417

Computation Systems Based on Hybrid Spin-wave–CMOS Integrated Architectures

SPIDER - Deliverable report

D6.1 - Report on spin-wave device and circuit behaviour

Disclaimer/ Acknowledgment

About SPIDER

In the future, the miniaturisation of electronic devices– epitomised by Moore's law – will be progressively limited by increasing power densities and the associated chip heating. Moreover, autonomous microelectronic applications, for example for the Internet of Things, demand high performance at ultralow power. Therefore, much research has recently focused on disruptive computing technologies that limit power consumption and optimise performance per circuit area. Spin wave computing is a disruptive spintronic technology that uses the interference of spin waves for computation and has considerable potential for power and area reduction per computing throughput. Despite much recent progress in the realisation of spin wave logic gates, no concept for a complete computing system exists today that is based only on spin waves. Thus, to advance from devices to systems, spin wave devices need to be complemented by CMOS in a hybrid spin wave–CMOS system. Using an interdisciplinary approach joining partners with expertise in materials science, physics, device manufacturing, electrical engineering, circuit design, and packaging, SPIDER targets the demonstration of a complete operational hybrid spin wave–CMOS computing system. To date, complex spin wave circuits are yet to be realised. SPIDER targets to fill this gap by developing spin wave logic circuits based on majority gates. To embed these circuits into a CMOS environment, SPIDER will design mixed signal CMOS chips that can drive spin wave circuits and read out computation results. The spin wave and CMOS chips will then be combined on an interposer to obtain the final hybrid system. This work will pave the way towards viable spin wave chips and provide a first benchmark of spin wave computing at the system level. Based on the results, SPIDER will then develop a roadmap to advance spin wave technology to compete with CMOS in technology nodes below 1 nm.

SPIDER consortium members

Document information

Deliverable No.	D6.1
Related WP	WP6
Deliverable Title	D6.1 - Report on SW device and circuit behaviour
Deliverable Date	01 – January - 2024
Deliverable Type	Report
Lead Author	Felix Kohl (RPTU)
Co-Author(s)	Philipp Pirro (RPTU), Florin Ciubotaru (IMEC)

Document history

Date	Revision	Prepared by	Approved by	Description
10/01/2024	1	Task Leader	WP leader	First draft
16/01/2024	2	WP Leader	Coordinator	Final

Dissemination level

PU	**Public**	x
SEN	**Sensitive**	

Publishable summary

We report on the first generation of YIG-based spin-wave devices produced in the SPIDER project which mainly serve to quantify the obtainable insertion loss and phase accumulation for the devices which will be connected to the CMOS chip. We show that the design of the spin-wave antennas to excite and detect the signals has an impact on the insertion loss (change about 3 dB). However, the thickness of the used YIG is impacting stronger (change about 5 dB with lower losses for thicker films). In addition, we investigate the antenna bandwidth and the power threshold above which insertion losses increase.

Contents

List of acronyms, abbreviations and definitions

Abbreviation	Definitions
WP	Work package
YIG	Yttrium iron garnet
GGG	Gadollinium gallium garnet
VNA	Vector-network-analyzer
CPW	Coplanar waveguide

1. Introduction

The computing primitive of the devices developed in SPIDER is based on the phase of propagating spin waves in magnonic microstructures. These structures are connected to the CMOS part via RF-to-magnon transducers in the form of microstructured RF antennas on top of the magnonic devices. The magnonic structures should have low RF insertion losses that only a small amount of amplification is required on the CMOS side. To allow for an easy integration, the insertion losses should not depend on the chosen input power for the targeted power range (around -30 dBm). In addition, the phase accumulation provided by the spin waves needs to be stable and on the order of 360°, which requires spin-wavelength in the micrometer range adjusted to the device length.

In this report, we present the results of 16 different spin-wave delay lines which constitute the basic building blocks of the spin-wave majority gates.

2. Spin-wave devices

2.1. Experimental setup

An inductive measurement method known as propagating spin-wave spectroscopy (PSWS) is used to investigate the spin-wave devices. The measurement setup used, and the measurement principle are described below.

The method of propagating spin-wave spectroscopy is based on the inductive excitation and detection of spin waves. The device under investigation is connected to a vector network analyzer (VNA) at port 1 and port 2 via commercial microwave probes (Picoprobe, GGB Industries). An RF voltage of known frequency is then applied to the input of the device from port 1. The flowing alternating current induces oscillating magnetic fields at the antenna, which in turn excite propagating spin waves in the magnetic medium under the antenna. If these propagate to the output of the device, the reverse process takes place. The oscillating magnetic stray fields of the spin wave induce an alternating current in the antenna at the output, which is detected by the VNA as an alternating voltage in magnitude and phase relative to the voltage coupled into port 1. The fraction of the signal transmitted in this manner from port 1 to port 2 is described by the scattering parameter S21. Parameter S12 is used for transmission in the opposite direction, from port 2 to port 1. By varying the frequency of the alternating voltage, the spectrum of the transmitted spin waves can be measured in magnitude and phase for given parameters. To remove the influence of the other elements in the microwave circuit, such as the cables and microwave probes, a short-open load-through calibration is carried out on a commercial calibration substrate before the measurements begin.

Since the spin wave spectrum of the magnetic medium depends not only on its material parameters but also on the magnitude and direction of the external magnetic field, the sample holder together with the sample and microwave probes is placed in an electromagnet to perform the measurements. The external field is oriented in the film plane parallel to the antennas. Consequently, spin-wave propagation is measured for the so-called Damon-Eshbach configuration where spin waves propagate perpendicular to the static magnetization (oriented parallel to the coplanar antennas). A Hall probe is attached close above the sample during the measurements, to monitor the magnitude of the applied external magnetic field during the measurement.

2.2. Sample layout and fabrication

The shape of the spin-wave antennas defines the wave vector range of the spin waves which can be excited. That is why different types of samples are produced for the systematic investigation of possible spin wave antenna layouts. The individual antenna structures were written on a YIG film into a lift-off mask of PMMA using electron lithography. Then a layer system of 10 nm titanium and 150 nm gold was deposited using electron beam evaporation.

The basic structure is identical for all devices. The core of each device consists of two identical coplanar waveguides arranged parallel to each other. They are produced on films of yttrium iron garnet

(YIG) of different thickness (100 nm, 200 nm, 400 nm, 800 nm) grown on a 500 µm gadolinium gallium garnet (GGG) substrate. The coplanar waveguides are each connected to bent contact pads to allow contact by means of the microwave probes. The scanning electron micrograph of an exemplary structure is shown in Figure 1.

Several parameters were varied over the entire sample series. Firstly, the entire mask was used on a total of four different YIG thicknesses in the range of 100 nm to 800 nm to investigate the influence of the YIG thickness on the performance of the device. In addition, coplanar waveguides with different layouts were applied to each sample of a thickness to investigate the influence of the CPW structure. Finally, the spacing between the two antennas, which constitutes the spin-wave propagation length, was varied from 10 µm to 70 µm to investigate the exponential decay length.

All different layouts of coplanar waveguides are chosen to efficiently excite spin waves of similar wavelengths. The excitation efficiency is given as a function of the wavelength from the spatial periodicity of the dynamic Oersted fields generated by the antenna. All four different types of antennas are listed in Table 1.

(a)   (b)
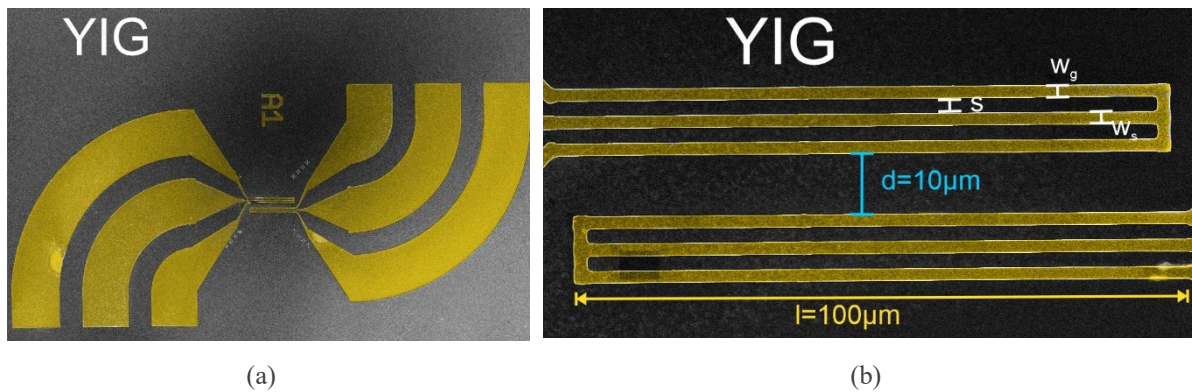
Figure 1: (a) Scanning electron microscope image of an exemplary spin-wave device. (b) Zoomed-in section of the CPW antennas for spin-wave excitation and detection. The antenna parameters s, w_g and w_s as well as the edge-to-edge distance of the CPS are indicated.

Table 1: Dimensions of ground line and signal line width and spacing for all different types of coplanar waveguides.

Type	w_g (µm)	s (µm)	w_s (µm)
1	2	2.5	2
2	1	2.5	2
3	2.5	2	2.5
4	1	4	1

2.3. Signal-to-noise ratio

A weak signal-to-noise ratio might be acceptable for experiments in the laboratory environment, as multi-stage measurement methods with many repetitions can be used for averaging. For the application in the SPIDER device however, this approach is not practicable, and the signal must be clearly

detectable, even in presence of a noisy background. For this reason, we have determined and quantified parameters influencing the ratio of signal strength to microwave background for the samples presented here. Possible controllable parameters that can be varied in the experiment are, for example, the external magnetic field, the type of antenna and the volume of magnetic material under the antenna, accessible via the length of the antenna but also the thickness of the magnetic material.

The matrix of scattering parameters for the two-port system of the VNA has been recorded for all different antennas on a total of four different thicknesses of YIG films, each for different magnetic field strengths, once resonant for spin wave excitation and once off-resonant to measure only the electric microwave background (unwanted leakage crosstalk) of the antennas. The measured frequency range has been estimated depending on the magnetic field to a frequency range around the expected resonance frequency of the spin waves.

For each microwave frequency, only spin waves of the same frequency are excited for a linear excitation process, provided that a spin wave mode exists for this frequency. For the investigated thin magnetic films magnetized in plane, this means that no propagating spin waves can be excited below a minimum frequency. In the case of the so-called Damon-Eshbach mode spin waves (blue curve in Fig. 2) considered here, this minimum frequency lies at spin waves of infinite wavelength/ vanishing wave vector k (so called Ferromagnetic Resonance, FMR). An exemplary dispersion relation for a 400 nm thick YIG film is shown in Figure 2. Due to the high thickness of the film, higher modes with a quantization along the film thickness (red lines) are also in the relevant frequency range. However, these higher modes hardly propagate due to their low group velocities. They are also excited much less efficiently by the antennas. Therefore, they do not contribute significantly to the transmission of the signal. However, they can influence it indirectly. Gaps in the otherwise continuous frequency spectrum, where there are no spin waves with sufficiently long wavelengths, form due to the avoided crossings of these modes with the fundamental modes (one avoided crossing is visible in Fig. 2 around 3.3 GHz). This can lead to dips in the transmission spectrum at these points.
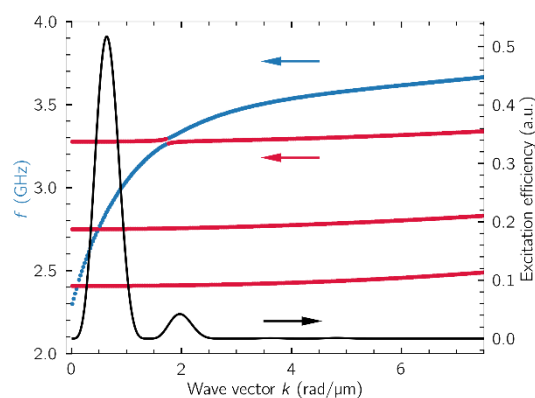
Figure 2: Dispersion relation for Damon-Eshbach spin wave modes in a 400 nm thick YIG film at an external field of 30 mT. The surface-wave-like mode is shown in blue, higher modes in red. The material parameters are A_{ex} = 3.5 pJ/m and M_s = 153 kA/m. In black the calculated excitation efficiency for the Damon-Eshabch mode for a CPW of type 1 is shown.

The excitation is additionally limited by the wavelength selectivity of the exciting CPW antenna (see excitation efficiency, black curve in Fig. 2). Due to the structure of the CPW, wavelengths with the same periodicity as the magnetic fields generated by the CPW are excited efficiently, while other

wavelengths cannot be excited at all. The usable frequency range of the spin wave device is therefore determined by the shape of the dispersion relation and the spatial distribution of the magnetic field of the CPW.

Figure 3 shows the obtained transmission parameters together with the off-resonant measured microwave background for an exemplary magnetic field at different YIG thicknesses. It can be seen directly from the figure that the ratio of signal strength to background increases significantly with increasing YIG thickness. From a thickness of 400 nm, the signal is so strong in relation to the directly transmitted microwave background that the spin wave signal can be clearly detected without the need for any multi-stage measurement process or additional averaging. Thus, concerning the signal-to-noise ratio, it would be best to choose the highest possible YIG thickness for future devices. Considering different magnetic field strengths and layouts of the coplanar waveguides provides qualitatively similar results. The thickness of the YIG was found to have the greatest influence on the devices used.
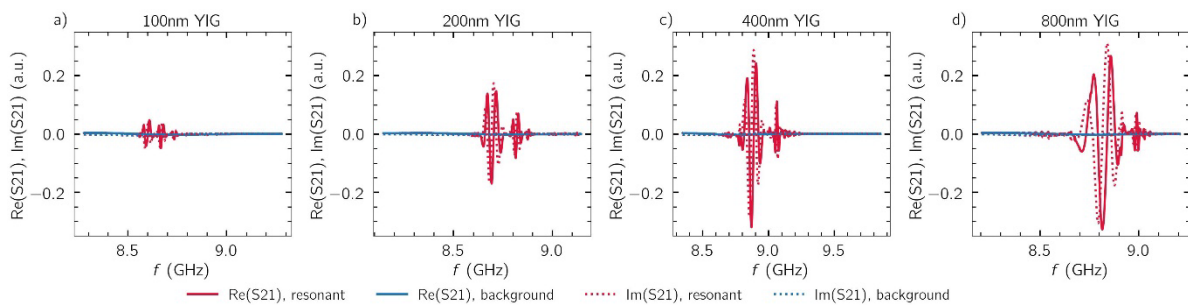
Figure 3: Transmission parameter measured for resonant and off-resonant excitation at an external field of 221 mT and an input power of -20 dBm for different YIG thickness from a) 100 nm to d) 800 nm and CPW of type 4.

To compare the influence of the different geometries of coplanar waveguides, the magnitudes of the measured transmission parameters for all different antenna types on 400 nm thick YIG for different external magnetic fields are shown in Fig. 4. In addition, the off-resonant microwave background is plotted. The latter shows a complex structure with local maxima and minima. This is attributed to a direct microwave cross talk of the contact pads and the CPW itself. Thus, this background is expected to look differently for the final structures since the microwave connection will be established via the interposer and a very different pad design. Across all tested magnetic fields and frequencies, a comparably large transmission signal is shown for each type of antenna. The signal-to-noise ratio varies in some cases due to the structure of the microwave background. For the thickest YIG, the signal-to-noise ratio is always greater than 30 dB and in the best case even 50 dB.
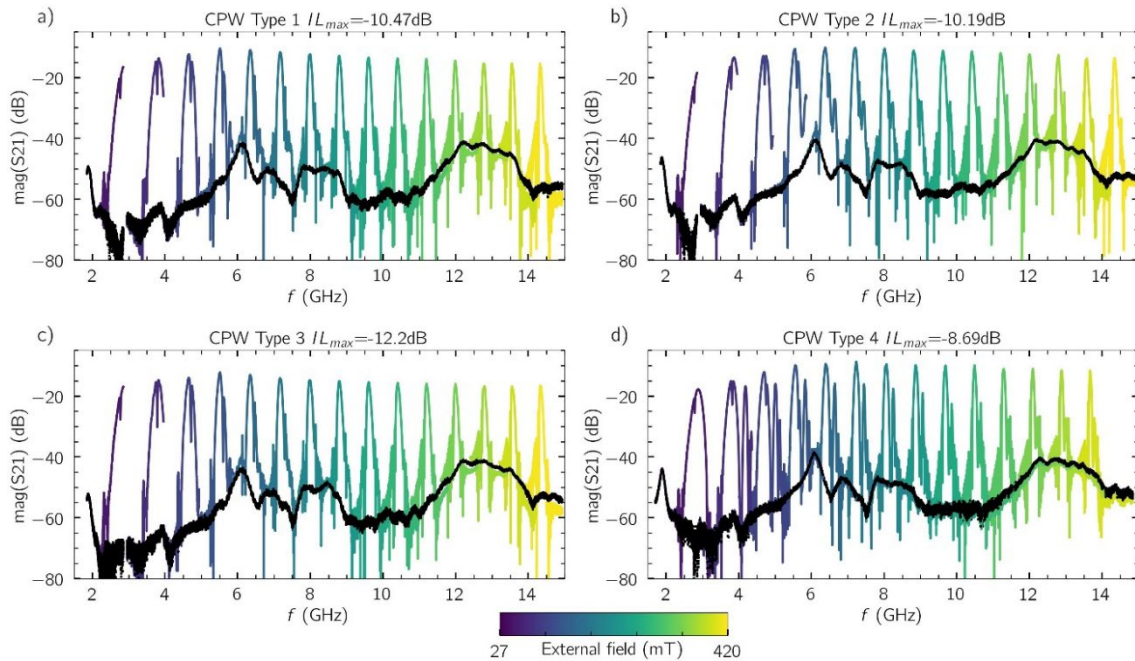
Figure 4: Measured magnitude of transmission parameter for the four different types of coplanar waveguides. Each peak corresponds to one external field value coded in colour and indicated by the color-bar at the bottom. The maximum achieved transmission L_{max} is indicated in each subfigure. The microwave background is shown as a black line.

However, there is a difference in the maximum transmission that can be achieved between the antennas. For the thickness of 400 nm YIG shown here, the maximum insertion loss is approximately 8.7dB for an input power of -20 dBm. In the case of the 800 nm thick YIG films, also for the type 4 antenna, the comparable value is even 7.6 dB. Such an insertion loss for on-chip microstructured antennas is, to the best of our knowledge, unprecedented in the literature and it illustrates the suitability of potentially further optimized spin-wave devices for practical applications.

2.4. Frequency bandwidth

In addition to the amplitude of the transmitted signal, other differences can also be determined for the various YIG thicknesses. In the experiment, for example, the excitation efficiency of the antenna does not depend directly on the frequency of the microwave, but on the spatial distribution of the antenna field. The efficiently excited range of wavelengths can then be translated into a frequency range via the dispersion relation of the spin waves. Depending on the YIG thickness, these differ significantly for the Damon-Eshbach mode. A comparison of the dispersions for a thickness of 100 nm and 800 nm YIG and the same parameters as for the previously calculated dispersions is shown in Figure 5.a. It can be seen directly from the figure that a larger frequency bandwidth is available for thicker YIG films due to the higher gradient (group velocity) in the used wave vector range. In principle, this allows a larger operational frequency range. However, the extent to which this is usable also depends on the efficiency of the excitation. A comparative measurement of the different YIG thicknesses is shown in Figure 5.b. First, it is noticeable that the frequency ranges for the individual thicknesses differ despite the same external magnetic field. This is also a direct consequence of the different slopes of the individual dispersion relations. Nevertheless, as already predicted by Figure 5.a, there is a clear difference in the

usable frequency range. It can therefore be concluded that high YIG thicknesses are preferred for devices which need a larger frequency bandwidth. This could be important for more complex majority gates that use frequency multiplexing to achieve higher data throughput.

(a)   (b)
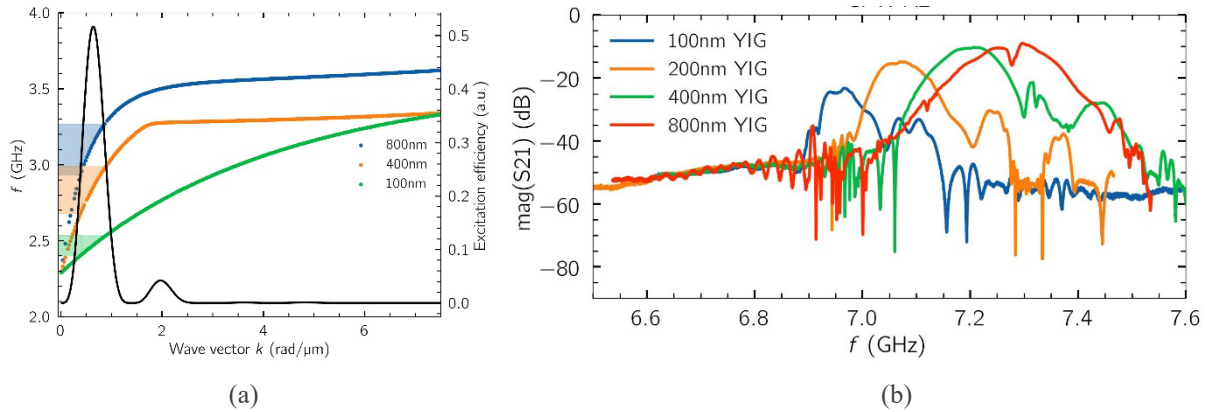
Figure 5: a) Dispersion relations for Damon-Eshbach spin-waves at an external field of 30 mT and different thicknesses. The shaded area marks for each dispersion the range of frequencies that can be excited. It is obtained from the FWHM of the antenna excitation efficiency, shown in black. b) Measured transmission spectrum S21 for different YIG thicknesses at an external field of 166 mT. The higher frequency bandwidth of the thicker YIG films is clearly visible.

2.5.   Power limits

In the first measurements, the magnetic field was varied for all measured devices at a low constant input power. However, the behavior as a function of the input power is also of interest for a future device, especially for the linear superposition of the different input spin waves, which is the basis of working principle of the majority gate. Since the input power level delivered from the CMOS chip to the spin-wave chip via the interposer must be adjusted depending on the insertion losses of the spin-wave chip and the output power levels, which in turn can be measured by the CMOS chip, it is important to quantify the linear operating range of the spin-wave chip. Outside this range, the insertion losses could increase substantially, or phase accumulation can be changed due to nonlinear spin-wave effects. To determine the linear working range, the input power is varied as an example for an identical device on all YIG thicknesses and one external field. Exemplary spectra obtained for a YIG thickness of 400 nm are shown in Figure 6.a. The measured off-resonant microwave background is constant (relative to the input power) over the input power. However, a different picture is found for the detected spin wave signal where a clearly different course is shown. As the input power increases, the ratio of spin wave transmission to microwave background decreases noticeably since the insertion losses increase. The absolute power transmitted by the spin waves still increases, but the absolute increase in transmission saturates. Also, the phase of the spin waves starts to change when powers above -9 dBm are applied. With the aid of micro-focused Brillouin light scattering measurements, the nonlinear excitation of other frequencies could be observed as a limiting effect for the power transmission at the same frequency as the excitation frequency. When detecting the signal exclusively at the excitation frequency, these represent an additional loss channel that only occurs when a threshold dependent on the excitation process is exceeded.

The measurement from Figure 6.a is repeated for the other YIG thicknesses. The maximum value of each spectrum obtained is extracted for each input power. A comparison can be found in Figure 6.b. There the obtained curves for different YIG thicknesses are shown. For all thicknesses, as already observed in Figure 6.a, there is a decreasing relative transmission for high powers. For low powers, on the other hand, the transmission is constant. The corresponding level is marked with a horizontal line. A high thickness of the YIG allows a higher power before non-linear effects limit it. This agrees with the interpretation that the deciding factor for spin-wave nonlinearities is the spin-wave energy density. Overall, the threshold for leaving the linear regime of spin-wave propagation lies significantly below 1 mW (0 dBm).

(a)   (b)
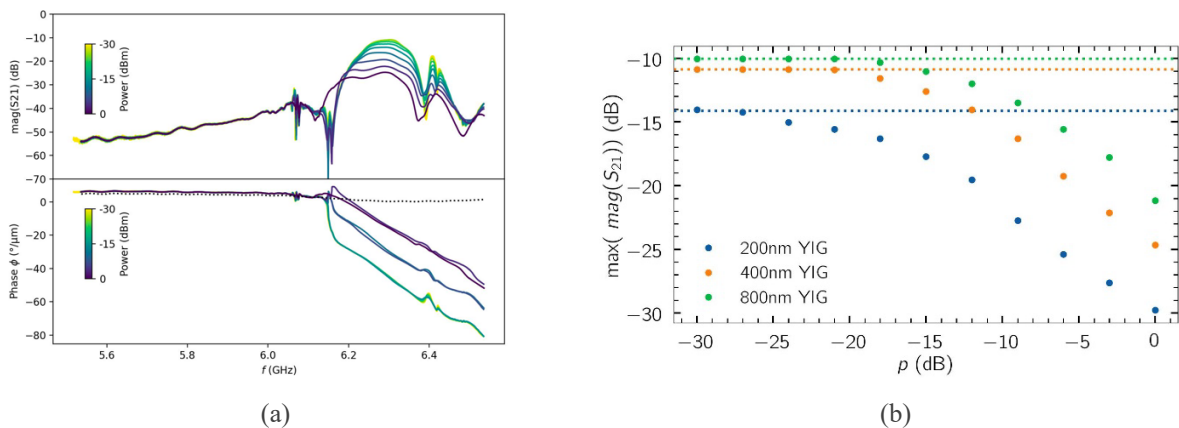
Figure 6: (a) Magnitude (top) and phase (bottom) of the measured S21 parameter for different input powers. The measurement is performed on 400 nm thick YIG at an external field of 139 mT. (b) Extracted maximum transmission parameter values relative to the input power for different YIG thicknesses (all measurements in Damon-Eshbach geometry).

To gain further insight into the physical origin of the limiting process, a micro-focused Brillouin light scattering spectroscopy measurement is carried out. For this purpose, a CPW of type 3 is contacted on the 400 nm thick YIG film. During the measurement, an external magnetic field of approximately 59 mT along the CPW direction is applied to the film. After a test measurement in which the excitation spectrum was recorded, the maximum of the excitation spectrum (approximately 3.64 GHz) is selected as the excitation frequency for the power-variant measurement. At low microwave power, only one peak is observed directly at the excitation frequency in the measured frequency spectrum of the scattered laser light. However, additional peaks occur as the power increases, one at lower frequency, two others close to the excitation frequency (see Figure 7.a). This is a clear indication of a nonlinear spin-wave propagation. For an inductive measurement with the VNA, these frequency-shifted signals are invisible, as only frequency components of the rf voltage with the same frequency as the output frequency of the VNA are acquired throughout the measurement process. However, these additional frequencies are disadvantageous for a potential spin wave majority gate, as they could still be detected by the sensing CPW. Therefore, their generation should be avoided if possible. To test whether this contribution is strong enough to explain the behaviour of the transmitted power limitation, the detected BLS intensity is extracted as a function of input power for all 4 peaks observed in Figure 7.a. Using a simple power law relationship for the BLS intensity as a function of RF power $\log_{10}(I) = 0.1 \cdot n \cdot P_{\mathrm{rf}} + a$, a slope of n = 1 is expected for a purely linear excitation. The fit to the data at low power for the main peak shows this behaviour. At high power the slope deviates, as already observed on the VNA. This is shown in

Figure 7.b. In addition, dips in the slope of the intensity of the main peak are also observed, and this deviation coincides exactly with the occurrence of the additional frequency peaks. This deviation from the linear curve also occurs at comparable power levels to the drop in transmitted power previously determined with the VNA for the 400 nm thick YIG. However, an exact comparison is not possible because the two setups use different microwave circuits and different rf probes to contact the sample and therefore have different absolute power transmissions to the CPW. Nevertheless, it can be concluded from the BLS measurement that frequency-converting non-linearities, known as magnon instabilities, are the limiting cause of power transmission in the current spin-wave devices.

(a)   (b)
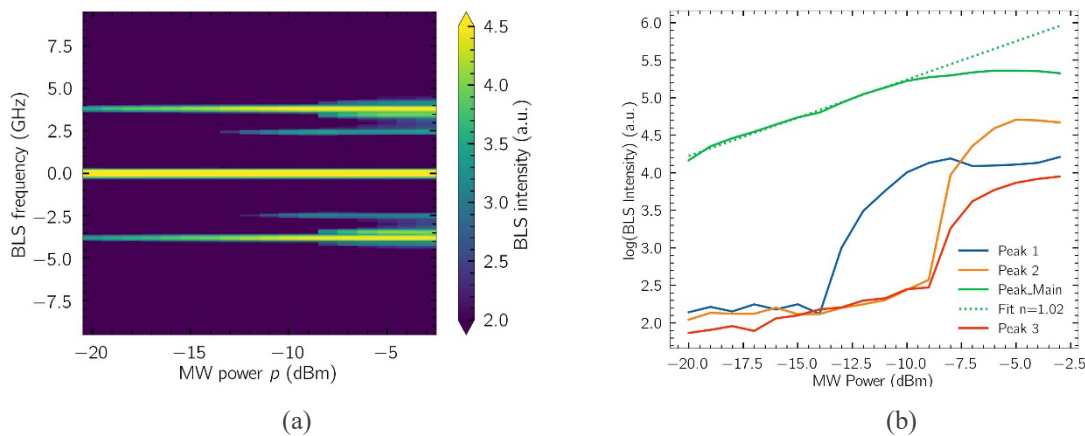
Figure 7: a) Measured BLS spectrum on 400 nm YIG for an external field of 59 mT and CPW type 3 in the middle between input and output CPW for different microwave powers. b) Extracted BLS intensities for the different peaks observed in part a).

2.6. Phase accumulation

So far, the magnitude of the signal transmitted by spin waves has been in the focus. However, the phase of the spin waves is of high importance since it is used as the signal carrier in the majority gate. In the transmission lines presented here, the output phase of a propagating spin wave depends on its frequency and the external magnetic field. The devices function as delay lines, which generate a time and thus a phase shift of a microwave inserted into the device. This results from the very low propagation speed of the spin waves compared to the group velocity of the microwaves and depends directly on the wavelength of a spin wave at a given frequency. As this is very small compared to microwaves of the same frequency (approximately 10 µm for the antennas used here), even very small propagation distances can lead to very large phase accumulation. For the majority gate design, it is important to verify that this phase accumulation is in the expected range and that it is stable and not disturbed, e.g. by the direct microwave crosstalk between the antennas, contact pads, etc. An exemplary accumulated unwrapped phase for spin-wave propagation and the respective background are shown in Figure 7. The phase is normalized to an effective propagation length of CPW-to-CPW center of 21 µm. At this point, the accumulated phase clearly illustrates how phase shifts can be generated even on a propagation path of a few µm in a device and that they are stable and in agreement with the expectations based on the calculated dispersion relations. The spin-wave induced phase shift, which is given by $\Phi = k(f) \cdot X$, (with X the distance between the antennas) increases with frequency since the wave vector k of the spin

waves increases with frequency for the Damon-Eshbach mode. The phase change gets steeper for high wave vectors since the group velocity starts to drop, which means that a given frequency interval is translated into a larger wave vector interval.

(a)   (b)
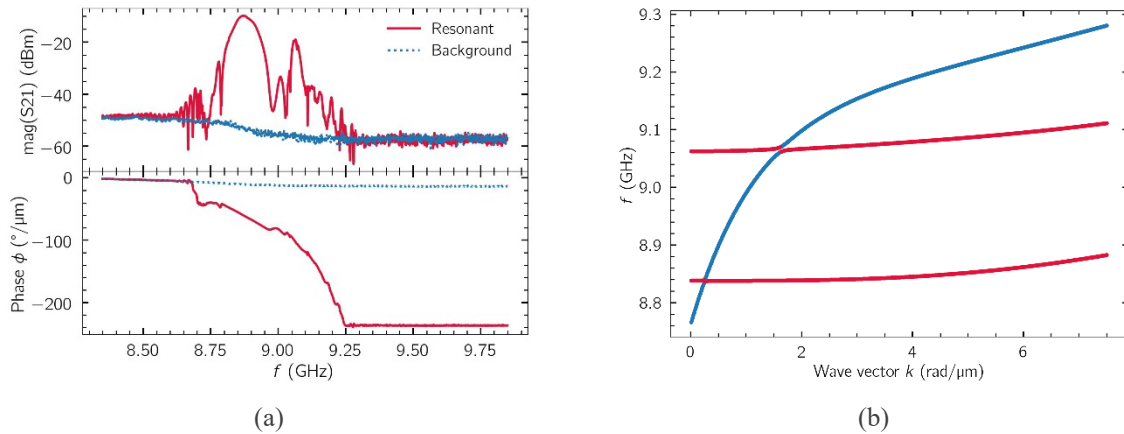
Figure 8: (a) Magnitude of transmission along with the unwrapped phases from VNA measurement for CPW type 4 on 400 nm YIG and an input power of -20 dBm at an external field of 226 mT. (b) Calculated dispersion relation for a 400 nm YIG film at an external field of 226 mT. The surface-wave like Damon-Eshbach mode is shown in blue, higher modes quatinzed along the thickness in red.

3.   Conclusions

The four chips of different YIG thicknesses with 16 spin-wave devices which we have fabricated show **low insertion losses (partially below 10 dB)**, **high signal-to-noise ratios (higher than 30 dB)** and a **linear working behaviour for input power levels below -20 dBm**. Thus, the envisioned device and antenna geometries are well suited to serve as the building blocks for practical spin-wave majority gates that can be interfaced with a mixed signal periphery.